15

Use of Acoustic Waves for Pulsating Water Jet Generation

Josef Foldyna
Institute of Geonics of the ASCR, v. v. i., Ostrava
Czech Republic

1. Introduction

The technology of a high-speed water jet cutting and disintegration of various materials attained considerable growth during the last decades. Continuous high-speed water jets are currently used in many industrial applications such as cutting of various materials, cleaning and removal of surface layers. However, despite the impressive advances made recently in the field of water jetting, substantial attention of number of research teams throughout the world is still paid to the improvement of the performance of the technology, its adaptation to environmental requirements and making it more beneficial from the economic point of view.

An obvious method of the water jetting performance improvement is to generate jets at ultra-high pressures. The feasibility of cutting metals with pure water jets at pressures close to 690 MPa was investigated already in early nineties of the last century (Raghavan & Ting, 1991). Such a high pressure, however, induces extreme overtension of high-pressure parts of the cutting system which has adverse effect on their lifetime.

An alternate approach, as shown in this chapter, is to eliminate the need for such high pressures by pulsing the jet. It is well known that the collision of a high-velocity liquid mass with a solid generates short high-pressure transients which can cause serious damage to the surface and interior of the target material. The liquid impact on a solid surface consists of two main stages (see Fig. 1). During the first stage, the liquid behaves in a compressible manner generating the so-called ''water-hammer'' pressures. These high pressures are responsible for most of the damage resulting from liquid impact on the solid surface. The situation shortly after the initial impact of the liquid on the solid surface is illustrated in Fig. 2. After the release of the impact pressure, the second stage of the liquid impact begins. Once incompressible stream line flow is established, the pressure on the central axis falls to the much lower Bernoulli stagnation pressure that lasts for relatively long time.

The force distribution on liquid jet impact on the solid surface can be summarized as follows: initially a small central area of the first contact is compressed under a uniform pressure. The magnitude of the impact pressure p_i on the central axis is given by

$$p_i = \frac{v\rho_1 c_1 \rho_2 c_2}{\rho_1 c_1 + \rho_2 c_2} \tag{1}$$

where v is the impact velocity and ρ_1, ρ_2 and c_1, c_2 are the densities and the shock velocities in the liquid and the solid, respectively (de Haller, 1933).

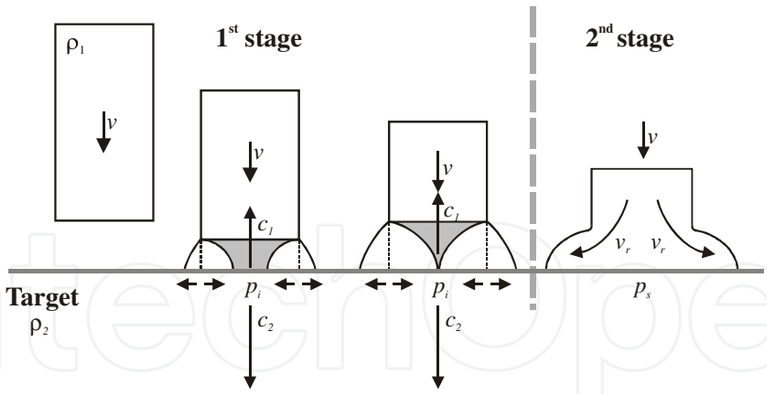

Fig. 1. Two stages of liquid impact on a solid target

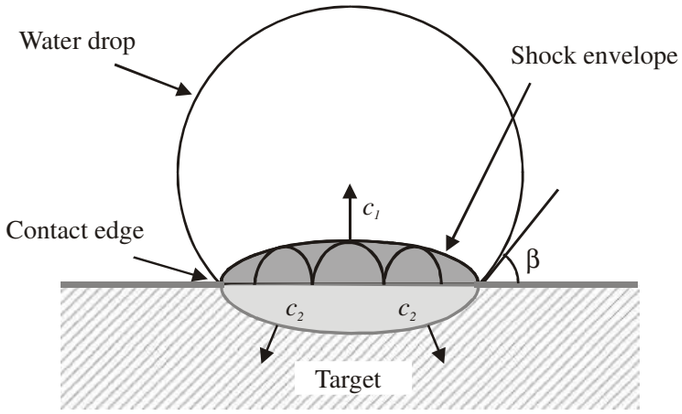

Fig. 2. Initial stage of impact between a water drop and a solid target with the contact edge moving faster than the shock velocity in the liquid. The liquid behind the shock envelope is compressed and the target beneath this area subjected to high pressure

The magnitude of the impact pressure is independent of the geometry of the drop (Thomas & Brunton, 1970), but the duration of the pressure is affected by the size and shape of the drop. For a sphere or cylinder the corresponding radius or half-width of the contact area R exposed to this pressure is given by

$$R = \frac{rv}{c_1} \tag{2}$$

where r is the radius of curvature of the drop or cylinder (liquid mass) in the region of contact (Bowden & Field, 1964).

The initial area of contact grows as the impact continues; there is very little reduction in pressure on the surface until appreciable outward flow begins. The outward flow of the liquid becomes possible when the limit of the compressible deformation of the liquid is exceeded. The limit is given by

$$\frac{v}{c_1} = sin\,\beta \tag{3}$$

where β is the liquid/solid interface angle – see Fig. 2 (Hancox & Brunton, 1966).

At this stage there is a rapid fall in pressure along the periphery of contact. As the outward flow continues, the water-hammer compression at the centre of impact is relieved until the maximum pressure acting on the surface is the central stagnation pressure for the incompressible flow. The stagnation pressure is given by

$$p_s = \frac{1}{2}\rho_1 v^2 \tag{4}$$

When the liquid begins to flow away from the point of impact, there is evidence that the velocity of this tangential flow may be as much as five times the impact velocity (Thomas & Brunton, 1970). The velocity increase is thought to be connected with the shape of the head of the jet. It has been observed that an increase in velocity along the surface occurs only in cases where the jet head is inclined at an angle to the surface. Since spherical drops (and/or spherical heads of a train of pulses of pulsating jet) always provide a sloping interface to a plane solid surface it might be expected that high radial velocities will occur on impact. Therefore, there are additional shear forces associated with the high speed flow across the surface acting on the surface in addition to the normal forces. The shear forces acting on a roughened surface are large enough to cause local shear fractures, even in high strength materials (Hancox & Brunton, 1966).

Exploitation of above described effects associated with water droplet impingement on solids in a high-speed water jet cutting technology should lead to considerable improvement of its performance, better adaptation to more and more demanding environmental requirements, and consequently to more beneficial use of the technology also from the economical point of view. Generating sufficiently high pressure pulsations in pressure water upstream the nozzle exit enables to create a pulsating water jet that emerges from the nozzle as a continuous jet and it forms into a train of pulses at certain standoff distance from the nozzle exit. Such a pulsating jet produces all of the above mentioned effects associated with water droplet impingement on solids. In addition, the action of pulsating jet induces also fatigue stress in the target material due to the cyclic loading of the target surface. This further improves the efficiency of the pulsating liquid jet in comparison with the continuous one. Thus, destructive effects of the continuous high-speed water jet can be enhanced by the introduction of high-frequency pulsations in the jet, i.e. by generation of pulsating water jets.

Recently, a special method of the generation of the high-speed pulsating water jet was developed and tested extensively under laboratory conditions. The method is based on the generation of acoustic waves by the action of the acoustic transducer on the pressure liquid and their transmission via pressure system to the nozzle. The high-pressure system with integrated acoustic generator of pressure pulsations consists of cylindrical acoustic chamber connected to the liquid waveguide. The liquid waveguide is fitted with pressure liquid supply and equipped with the nozzle at the end. The acoustic actuator consisting of piezoelectric transducer and cylindrical waveguide is placed in the acoustic chamber (see Fig. 3). Pressure pulsations generated by acoustic actuator in acoustic chamber filled with pressure liquid are amplified by mechanical amplifier of pulsations and transferred by liquid waveguide to the nozzle. Liquid compressibility and tuning of the acoustic system are utilized for effective transfer of pulsating energy from the generator to the nozzle and/or nozzle system where pressure pulsations transform into velocity pulsations. The acoustic generator can be used for generation of both single and multiple pulsating water jets (e.g.

rotating) using commercially available cutting heads and jetting tools. Laboratory tests of the device based on the above mentioned method of the pulsating liquid jet generation proved that the performance of pulsating water jets in cutting of various materials is at least two times higher compared to that obtained using continuous ones under the same working conditions.

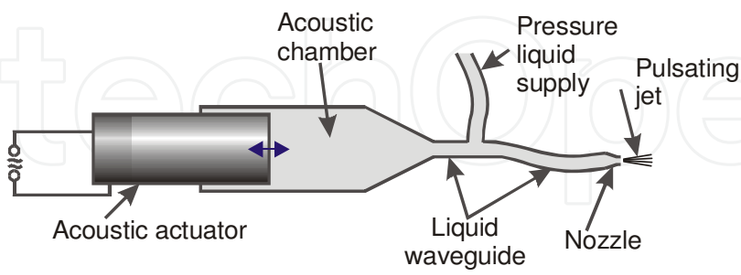

Fig. 3. Schematic drawing of the high-pressure system with integrated acoustic generator of pressure pulsations

However, further improvement of the apparatus for acoustic generation of pulsating liquid jet requires thorough study oriented at determination of fundamentals of the process of excitation and propagation of acoustic waves (and/or high-frequency pressure pulsations) in liquid via high-pressure system and their influence on forming and properties of pulsating liquid jet.

Problems related to the generation and propagation of pressure pulsations with frequency in the order of tens of kHz in liquid under pressure of tens of MPa and subsequent discharge of the liquid influenced by the pulsations through the orifice in the air (producing pulsating liquid jet with axial velocity in the order of hundreds meters per second) were not investigated in detail so far. Only partial information on this topic can be found in publications dealing with processes of a fuel injection for combustion in diesel engines (see e.g. Pianthong et al., 2003 or Tsai et al., 1999) and/or underwater acoustics (Wong & Zhu, 1995).

Therefore, the research on pulsating water jets was focused recently on the study of fundamentals of the process of excitation and propagation of acoustic waves (high-frequency pressure pulsations) in liquid via high-pressure system and their influence on forming and properties of pulsating liquid jet as well as on the visualization of the pulsating jets and testing of their effects on various materials. Results obtained in above mentioned areas so far are summarized in following sections.

2. Acoustic wave propagation in high-pressure system with integrated acoustic generator

The efficient transfer of the high-frequency pulsation energy in the high-pressure system to longer distances represents one of the basic assumptions for generation of highly effective pulsating water jets with required properties. To achieve that goal, the amplification of pressure pulsations propagating through the high-pressure system is necessary. The amplification can be accomplished by properly shaped liquid waveguide that is used for the pulsations transfer to the nozzle. In addition, maximum effects will be obtained if the entire high-pressure system from the acoustic generator to the nozzle is tuned in the resonance. To

be able to study theoretically process of generating and propagation of pressure pulsations in the high-pressure system, both analytical and numerical models of the system with integrated acoustic generator were developed.

2.1 Analytical solution

The analytical solution of both pressure and flow oscillation waveforms in the conffuser-shaped tube with circular cross-section is based on linearized Navier-Stokes equations and wave equation for propagation of pressure wave. The wave equation incorporates both the standard kinematical viscosity and the kinematical second viscosity that is related to the liquid compressibility. Therefore, the irreversible stress tensor Π_{ij}, on the basis of which the wave equation is derived, can be written as follows:

$$\Pi_{ij} = 2\eta c_{ij} + \delta_{ij} \int_0^t \Theta(t-\tau) c_{kk}(\tau) d\tau \tag{5}$$

where the function Θ (dynamic second viscosity) is related to the voluminous memory, and c_{ij} represents the tensor of deformation velocity.
In the frequency domain (ω), equation (5) can be written in simplified form verified experimentally:

$$\Pi_{ij\omega} = 2\eta c_{ij\omega} + \delta_{ij} \frac{k}{\omega} c_{kk\omega} \tag{6}$$

whereby δ_{ij} represents Kronecker delta, and η dynamic viscosity. It is obvious from (6) that the dynamic second viscosity is frequency dependent. The kinematical second viscosity is then defined using following formula:

$$\xi = \frac{k}{\rho\omega} \tag{7}$$

where ρ represents liquid density.

2.1.1 Wave equation

If one considers linearized Navier-Stokes equations, the wave equation for pressure function can be written using the Laplace operator Δ in the following form:

$$\frac{\partial^2 p}{\partial t^2} - 2\gamma \frac{\partial}{\partial t}(\Delta p) - \int_0^t \rho^{-1} \Theta(t-\tau) \frac{\partial}{\partial \tau}(\Delta p)\, d\tau - v^2 \Delta p = 0 \tag{8}$$

where γ is kinematical viscosity, p pressure, t time and v speed of sound in water, respectively.
If Laplace transformation for zero initial conditions is applied in (8), following equation can be obtained:

$$s^2\sigma - s[2\gamma + \xi(s)]\Delta\sigma - v^2\Delta\sigma = 0 \tag{9}$$

where s represents parameter of the Laplace transformation according to time ($\xi(s)$ is the Laplace function of the second kinematical viscosity), and, at the same time, following is valid:

$$L\{p(t)\} = \sigma(s) \tag{10}$$

If following expression is denoted κ:

$$\kappa^2 = -s^2[v^2 + (2\gamma + \xi)]^{-1} \tag{11}$$

then it can be written

$$\kappa^2\sigma + \Delta\sigma = 0 \tag{12}$$

In the frequency domain it is valid that $\psi(i\omega) = k/\omega$.
The solution of (12) can be performed by the implementation of spherical coordinate system (r, φ, υ), see Fig. 4. Now, the wave equation can be written in the following form:

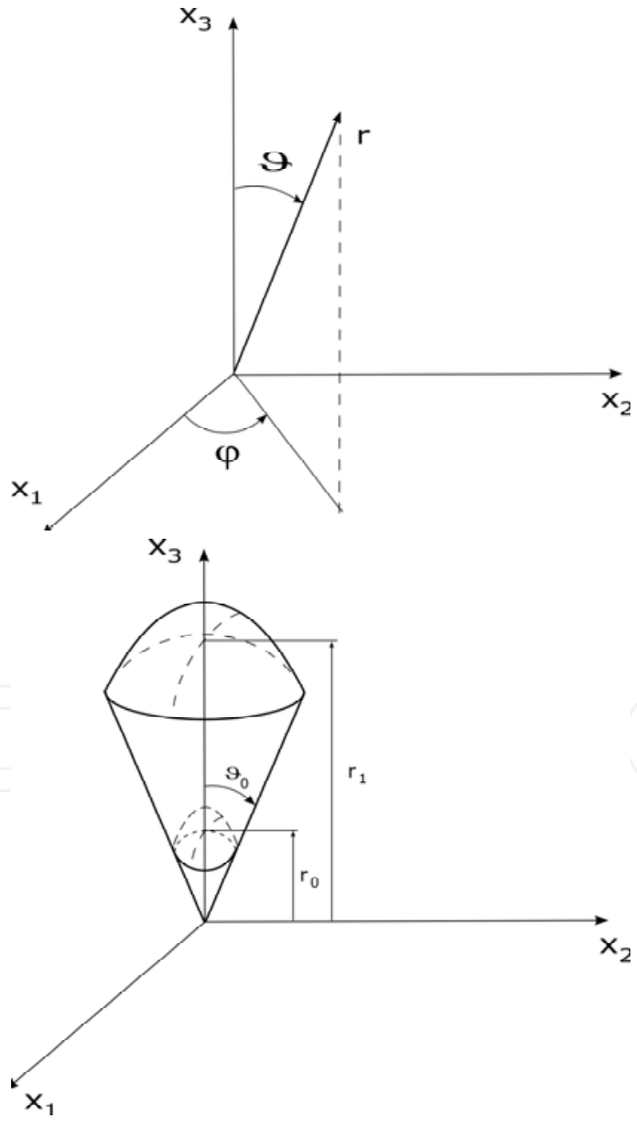

Fig. 4. Implementation of spherical coordinate system

$$\frac{\partial^2\sigma}{\partial r^2}+\frac{2}{r}\frac{\partial\sigma}{\partial r}+\frac{1}{r^2}\frac{\partial^2\sigma}{\partial \upsilon^2}+\frac{1}{r^2}\mathrm{cotg}\frac{\partial\sigma}{\partial \upsilon}+\frac{1}{r^2}\frac{1}{\sin^2\upsilon}\frac{\partial^2\sigma}{\partial\varphi^2}+\kappa^2\sigma=0 \tag{13}$$

Let's assume the solution of (13) as a product of functions:

$$\sigma = Z(r)W(\cos\upsilon)\Phi(\varphi) \tag{14}$$

Then, individual particular integrals can be expressed as follows:

$$\Phi_p = A_n\cos n\varphi + B_n\sin n\varphi \tag{15}$$

$$W_p(\cos\upsilon) = M_{nm}P_m^n(\cos\upsilon) + N_{nm}Q_m^n(\cos\upsilon) \tag{16}$$

where *P, Q* are special Legendre polynomials:

$$\mathrm{Z}_p = \frac{1}{\sqrt{r}}[F_mJ_D(\kappa r)+G_mY_D(\kappa r)] \tag{17}$$

$$D = \frac{\sqrt{1+4m(m+1)}}{2} \tag{18}$$

2.1.2 Transfer matrix

The objective is to determine transfer matrix $\boldsymbol{P}$ that can be used in solving pressure and flow pulsations in hydraulic systems in conffuser-type tubes. For this purpose, it is convenient to introduce the mean velocity of the liquid c_r in a direction of r using following formula:

$$\widetilde{c_r} = \frac{1}{2\upsilon_0}\int_0^{\upsilon_0} c_r(r,\varphi,\upsilon)d\upsilon \tag{19}$$

The solution can be simplified by the assumption that the flow is rotary symmetrical. It can be derived under the above mentioned assumption that functions P_m^n, Q_m^n will be streamlined to the following form: P_m^0, Q_m^0. Further, considering that the pressure function p varies only a little with respect to the angle υ, the following relation for the mean velocity c_r can be written based on Navier-Stokes equations:

$$\frac{\partial\widetilde{c_r}}{\partial t} = -\frac{2\upsilon_0}{\rho}\frac{\partial p}{\partial r}-\frac{2\upsilon_0\xi}{\rho^2\nu^2}\frac{\partial^2 p}{\partial r\partial t} \tag{20}$$

The continuity equation and component c_r in Navier-Stokes equations expressed in the spherical coordinate system were used in the above mentioned derivation. Withal, effects of dynamic viscosity were neglected. If we will keep considering zero initial conditions, it can be written after the Laplace transformation (20):

$$sw_r = \alpha\frac{\partial\sigma}{\partial r}; L\{\widetilde{c_r}(t)\} = w_r(s) \tag{21}$$

$$\alpha = -\frac{2\upsilon_0}{\rho}\left(1 + \frac{s\xi}{v^2}\right) \tag{22}$$

If all assumptions of the solution are considered, following can be written for Laplace images of both the pressure function and the velocity $\widetilde{c_r}$ and with respect to (21):

$$\sigma = \frac{1}{\sqrt{r}}[FJ_{0.5}(\kappa r) + GY_{0.5}(\kappa r)] \tag{23}$$

$$m = 0;\ D = \frac{1}{2} \tag{24}$$

$$w_r = \frac{\alpha}{s\sqrt{r}}\left[F\frac{\partial J_{0.5}(\kappa r)}{\partial \gamma} + G\frac{\partial Y_{0.5}}{\partial r}\right] \tag{25}$$

If we introduce for $r = r_0$ the state vector

$$\mathbf{u}^T = [w_r(r_0, s), \sigma(r_0, s)] \tag{26}$$

and for *r* the state vector

$$\mathbf{u}^T = [w_r(r, s), \sigma(r, s)] \tag{27}$$

the dependence in locations *r* and r_0 can be expressed by means of the transfer matrix:

$$\mathbf{u}(r, s) = \mathbf{P}\mathbf{u}(r_0, s) \tag{28}$$

Then, the matrix **P** will be derived from (26) and (27) by the elimination of integration constants *F*, *G*. If we designate:

$$\delta = \frac{\alpha}{r}\left[\frac{\partial J_{0.5}}{\partial r}(\kappa r_0)Y_0(\kappa r_0) - \frac{\partial Y_{0.5}}{\partial r}(\kappa r_0)J_{0.5}(\kappa r_0)\right] \tag{29}$$

following relation can be written for matrix **P**:

$$\mathbf{P} = \frac{1}{\delta\sqrt{r_0 r}}\begin{Vmatrix} \alpha\frac{\partial J_{0.5}}{\partial r}(\kappa r) & \alpha\frac{\partial Y_{0.5}}{\partial r}(\kappa r) \\ J_{0.5}(\kappa r) & Y_{0.5}(\kappa r) \end{Vmatrix}\begin{Vmatrix} Y_0(\kappa r_0) & -\alpha\frac{\partial Y_{0.5}(\kappa r_0)}{\partial r} \\ -J_{0.5}(\kappa r_0) & \alpha\frac{\partial J_{0.5}}{\partial r}(\kappa r_0) \end{Vmatrix} \tag{30}$$

In the frequency domain, $s = i\omega$ is substituted.

Both pressure and flow pulsations of hydraulic systems with conffuser-shaped tubes can be solved on the basis of the transfer matrix (30). Individual elements of the transfer matrix are dependent on values of the speed of sound and the second viscosity. Values of both these quantities depend on the static pressure and the value of second viscosity depends also on the frequency. The values can be determined experimentally using the transfer matrix.

2.1.3 Application of the transfer matrix

The transfer matrix derived in the previous section can be used in solving transmission of pressure and flow pulsations in complex hydraulic systems. Such a system can consist of cylindrical and confusser-shaped sections; the system can also be bifurcated.

The advantages of use of the transfer matrixes for determination of both pressure and flow oscillation waveforms in the hydraulic system are illustrated on the model of the conffuser-shaped tube with the circular cross-section. The tube consists of series of coaxial cylinders with various diameters connected with cone frustums and filled with water at a pressure of 30 MPa. The acoustic generator of pressure pulsations located at the end of the largest diameter cylinder vibrates at the frequency of 20 kHz. The cylindrical nozzle is situated on the other end of the tube. The length of the largest diameter cylinder L_1 (and thus also total length of the tube L) can be changed (see Fig. 5).

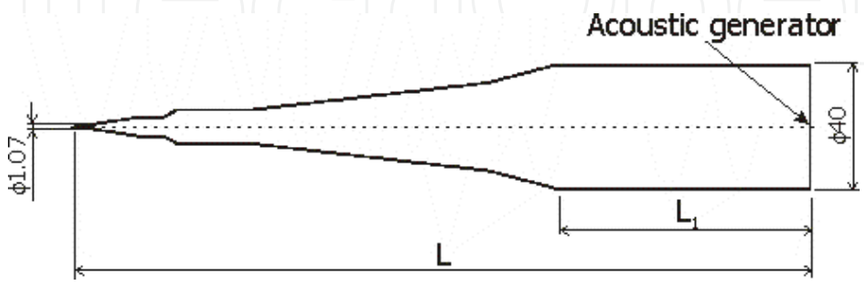

Fig. 5. Schematic drawing of the conffuser-shaped tube with circular cross-section

Effects of acoustic generator on the pressurized fluid in the tube are simulated by mean velocity:

$$\widetilde{c_r} = c_{r0}e^{i\omega t}; w_{r0} = \frac{1}{s - i\omega} \tag{31}$$

The cylindrical nozzle at the end of the conffuser is represented by the linear hydraulic resistance, simulated by following equations:

$$p = \lambda c_r;\ \sigma = \lambda w_r \tag{32}$$

where λ represents the discharge coefficient.

Based on the transfer matrixes, a simulation model with the above described geometrical configuration was elaborated. Firstly, the natural frequency of the hydraulic system in question was determined using the simulation model. Next, the frequency was applied as oscillation frequency of the acoustic generator and propagation of a generated forced pressure waveform in the hydraulic system was investigated. Fig. 6 illustrates calculated forced pressure waveforms in the simulated geometry related to the phase angle.

It can be seen from the Fig. 6 that oscillations of the acoustic actuator generate a standing wave in the hydraulic system. The standing wave converts to the travelling wave at the area close to the nozzle exit. It is obvious from the presented solution that a properly designed conffuser-type tube can amplify the amplitude of pressure pulsations at the exit of the pulsating nozzle.

The presented analytical solution of the problem of the acoustic (pressure) wave propagation in the high-pressure system can be used for the determination of the optimal geometrical configuration of the high-pressure system to operate in the resonance mode. The solution can also be used in design of a transmission line for efficient transfer of high-frequency pulsation energy to longer distances in high-pressure systems for generation of pulsating high-speed water jets.

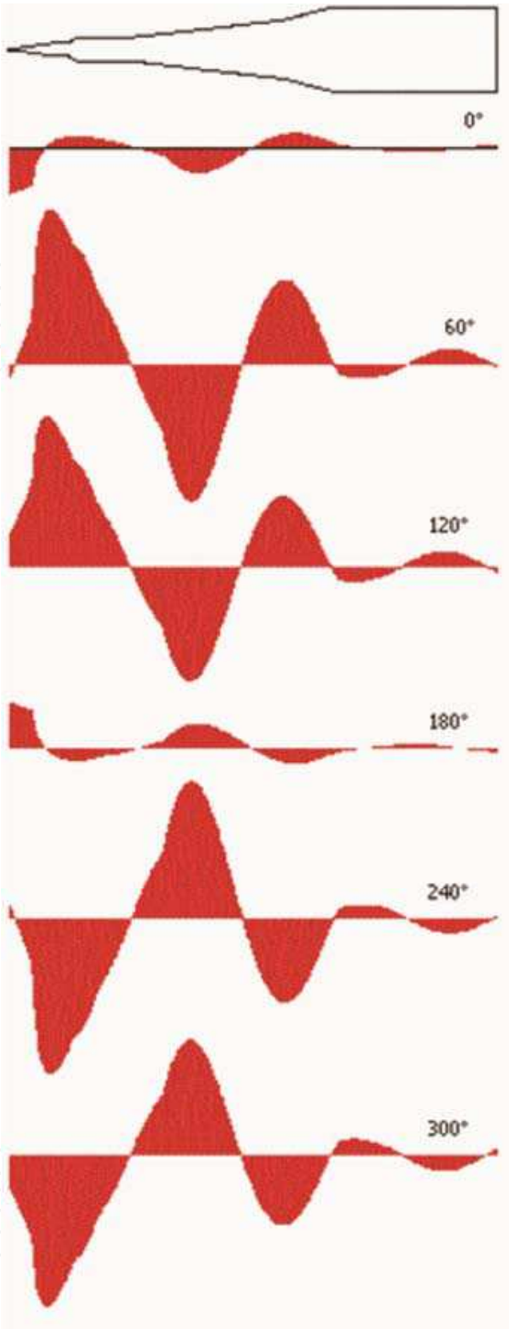

Fig. 6. Amplitudes of forced pressure waveforms in the simulated geometry related to the phase angle calculated from the analytical model

2.2 Numerical model

Computational Fluid Dynamics (CFD) models of selected geometrical configurations of the high-pressure system with integrated acoustic generator were created using CFD code ANSYS CFD to simulate numerically the influence of operating and configuration parameters of the acoustic generator and transmitting line on the generation and

propagation of acoustic waves (pressure pulsations) in high-pressure system and properties of pulsating jet. The high-pressure system consisted of cylindrical acoustic chamber, liquid waveguide provided with high-pressure water supply and the nozzle. To simplify the model, acoustic actuator was substituted by vibrating wall of the acoustic chamber. The fluid flow in the model was solved as 3-D turbulent compressible unsteady flow of water. Water compressibility was taken into account in the numerical model using so called user defined function (UDF). The UDF covers calculations of both water density and speed of sound in water related to pressure:

$$\rho = \frac{\rho_{ref}}{1 - \frac{\Delta p}{K}} = \frac{\rho_{ref}}{1 - \frac{p - p_{op}}{K}} \tag{33}$$

$$a = 2.10^{-6}p + 1432 \tag{34}$$

where ρ is water density [kg.m^{-3}], ρ_{ref} is reference water density under normal conditions (998,2 kg.m^{-3}), p and p_{op} are real and operating pressures [Pa], K represents bulk modulus of water (2.2 . 10^9 Pa) and a is speed of sound in water [m.s^{-1}] determined experimentally.
The numerical simulation of a high-pressure system equipped with an acoustic generator was verified by the measurement of pressure pulsations in the high-pressure system upstream to the nozzle exit using dynamic pressure sensors. The pressure waveform in the numerical model was recorded at the same location as the pressure sensor was installed during the laboratory measurement. It was found out that numerical model provides information on the pressure waveform in high-pressure system that is in relatively very good agreement with experimental measurement. Comparison of results of numerical simulation and measurement also proved that the numerical model is able to simulate influence of geometry changes on the amplitude of dynamic pressure accurately and thus also to simulate pressure wave propagation and transmission in the high-pressure system.

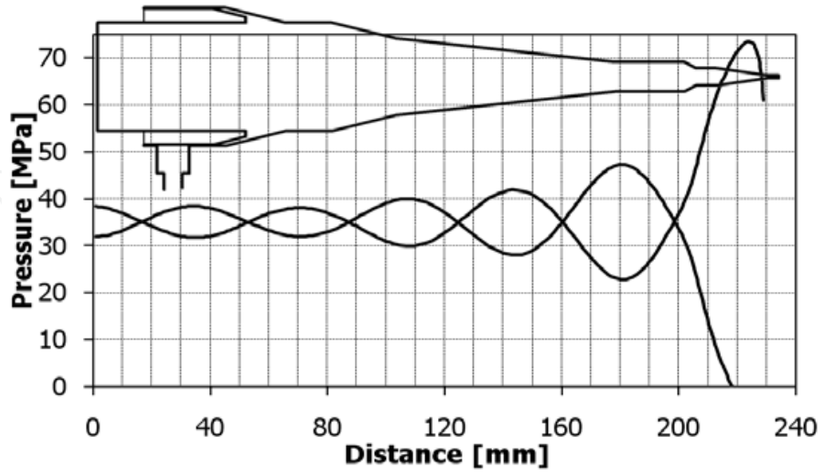

Fig. 7. Standing wave amplitudes along longitudinal axis of the high-pressure system

After the verification of plausibility of results of numerical simulation by the laboratory measurement, the model was used in studying of the process of propagation and transmission of acoustic waves in the high-pressure system from the acoustic actuator to the

nozzle. An example of the behaviour of amplitudes of standing wave along the longitudinal axis of high-pressure system can be seen in Fig. 7. Figure 8 illustrates forced pressure waveforms in the simulated geometry related to the phase angle.

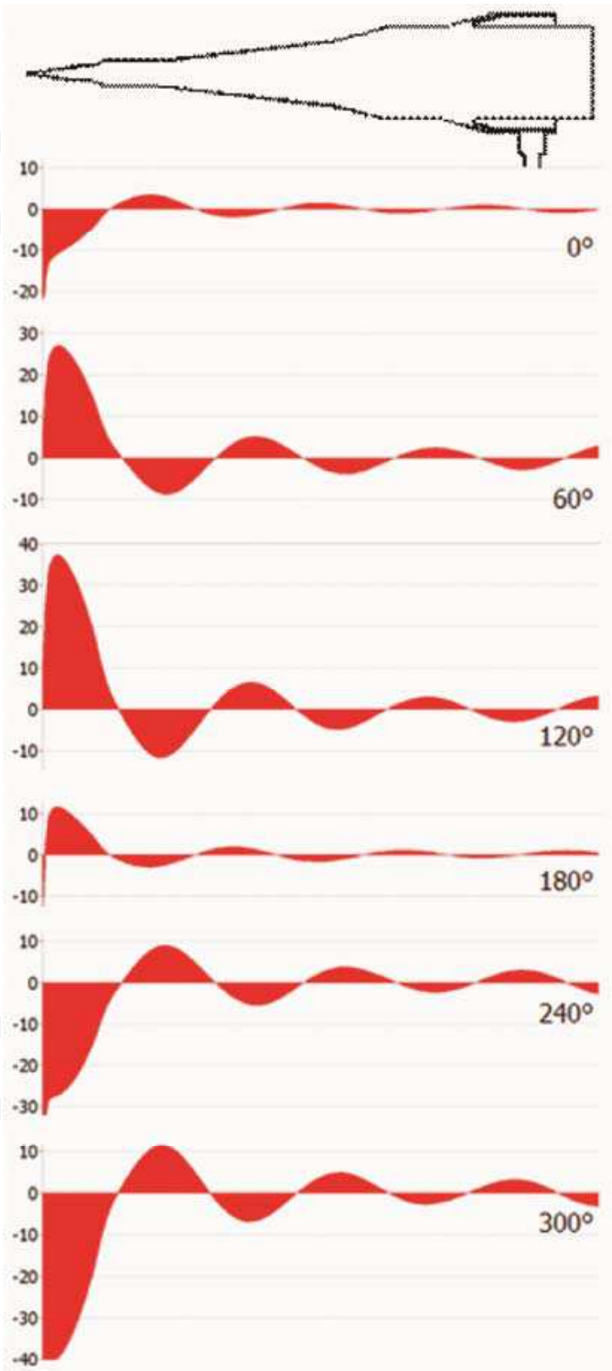

Fig. 8. Calculated forced pressure waveforms in the simulated geometry related to the phase angle recorded along the longitudinal axis of high-pressure system – from numerical model. (Scale indicates amplitude of dynamic pressure in MPa.)

Results obtained from the numerical simulation correspond to results obtained from the analytical one even if the numerical model used is not physically accurate in the close vicinity of the nozzle outlet where cavitation occurs. Cavitation model was not implemented in the numerical model with respect to the computational speed. Results of numerical modelling clearly indicate that the geometrical configuration of high-pressure system influences significantly propagation and transmission of pressure pulsations from the acoustic actuator to the nozzle. The amplitude of pressure waves increases towards the nozzle outlet due to the proper shaping of the liquid waveguide – its frustums act as mechanical amplifiers of the acoustic waves. At the same time, the amplitude of pressure pulsations close to the nozzle outlet (where it has crucial influence on the pulsating jet generation) changes significantly with respect to the geometrical configuration of the high-pressure system.

3. Visualization of pulsating jet

The use of visualization plays an important role in the study of behaviour of pulsating water jet. It enables not only the examination of characteristics of the jet such as mean velocity and break-up length of the pulsating jet but also to study the morphology and processes of formation of the pulsating jet and development of pulses in the jet. Furthermore, the visualization can be used to validate results obtained from numerical simulation of the process of generation of pulsating jets using CFD methods.
An original method of visualization of pulsating water jets based on the application of stroboscopic effect was elaborated for the above mentioned purposes. The method enables to obtain visual information not only on instantaneous structure of the pulsating jet but also on the mean structure of the jet. In addition, the stroboscopic effect allows observing process of formation of pulsating water jet by the naked eye. Special stroboscope for the pulsating jet visualization was developed where the frequency of stroboscope flashing is controlled by the frequency of pressure pulsations in the high-pressure system measured upstream from the nozzle exit. An example of the mean structure of pulsating jet with pulsating frequency of 20 kHz can be seen in Fig. 9. Exposure time of the photograph was 1/1000 s and the frequency of stroboscope flashing was about 20 kHz, therefore the figure represents superposition of 20 images of pulsating jet "frozen" by the stroboscope flashing.

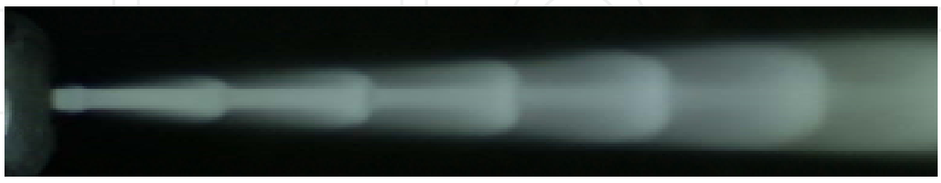

Fig. 9. The mean structure of the pulsating water jet generated at 30 MPa (illumination by the stroboscope)

An instantaneous structure of the pulsating water jet with the frequency of 20 kHz was studied using the high-speed camera LaVision VC-HighSpeedStar 5 equipped with image amplifier LaVision HighSpeed IRO. The record rate of the high-speed camera was 35 000 frames per second and the gate was set to 1μs. In addition, visualization of instantaneous structure of the pulsating water jet was also performed using Particle Image Velocimetry (PIV) system consisting of LaVision Imager Intense camera and New Wave Research laser,

Model Solo 120 with pulse duration 3-5 ns; the optical system was used to produce 1 mm thick sheet of light. An example of the pulsating jet visualized by high-speed camera can be seen in Fig. 10, the same jet visualized by PIV system is presented in Fig. 11.

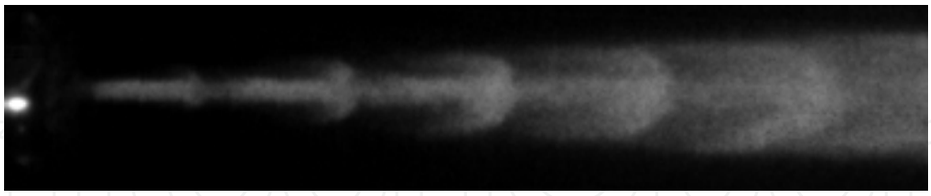

Fig. 10. The instantaneous structure of the pulsating water jet generated at 30 MPa (high-speed camera)

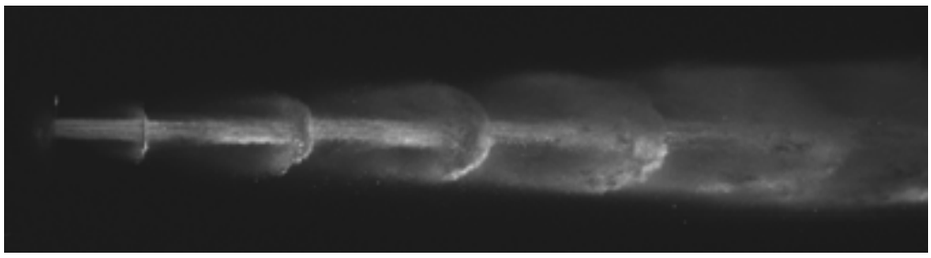

Fig. 11. The instantaneous structure of the pulsating water jet generated at 30 MPa (PIV system)

The fan (flat) pulsating water jet visualization was performed using the pulsed laser New Wave Research and digital camera Nikon D70s. Figure 12 shows the morphology of fan pulsating water jet generated at a pressure of 20 MPa.

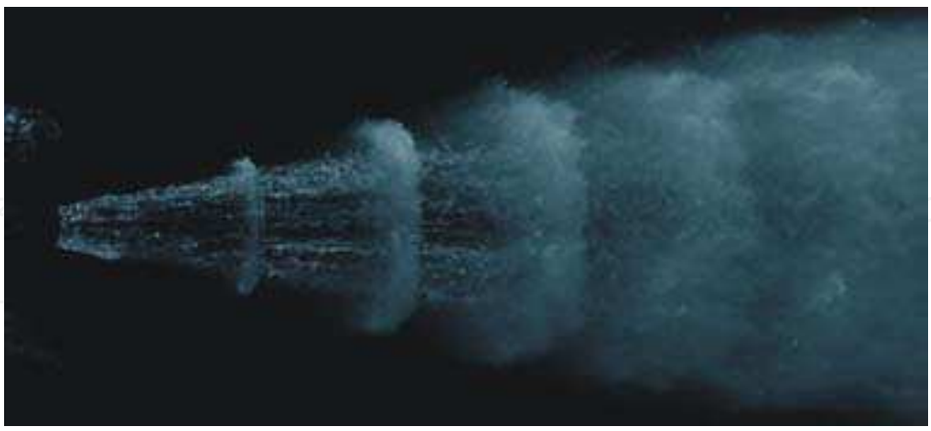

Fig. 12. The instantaneous structure of the fan pulsating water jet generated at 20 MPa (illumination by pulsed laser, camera Nikon D70s)

4. Effects of pulsating water jets on materials

Effects of pulsating water jets with the frequency of 20 kHz were tested on various types of materials, such as metals, rocks and concrete. Tested materials were exposed to the action of

diverse types of jets: single round and fan pulsating jets as well as rotating pulsating jets. The effects of pulsating jets were evaluated in terms of cutting depth, rate of mass-loss or volume removal rate respectively and compared with the effects of continuous water jets under the same operating conditions.

Obtained results show clearly the supremacy of pulsating water jets over continuous ones in terms of their effects on material. Figures 13 to 15 illustrate the effects of various types of both pulsating and continuous jets on metal, rock and concrete samples. Differences in the surface structures created by pulsating and continuous water jets on individual materials are clearly visible in the above mentioned figures. An example of erosion effects of pulsating fan water jets (generated at various pressures) on aluminium samples at variable stand-off distance is presented in Figure 16.

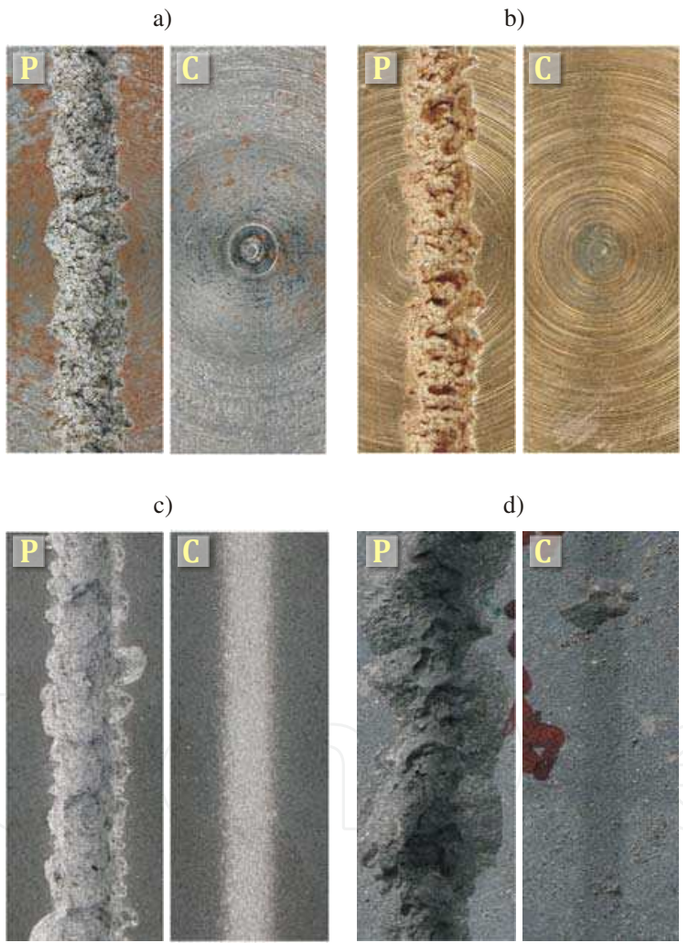

Fig. 13. Comparison of effects of pulsating (P) and continuous (C) water jets on samples of: a) mild steel (pressure 40 MPa, nozzle dia. 1.98 mm, traverse speed 0.03 m.min^{-1}, standoff distance 140 mm), b) brass (pressure 40 MPa, nozzle dia. 1.98 mm, traverse speed 0.03 m.min^{-1}, standoff distance 140 mm), c) duralumin (pressure 50 MPa, nozzle diameter 1.45 mm, traversing speed 0.05 m.min^{-1}, standoff distance 60 mm) and d) basalt (pressure 50 MPa, nozzle diameter 1.45 mm, traversing speed 1.0 m.min^{-1}, standoff distance 40 mm (P) and 20 mm (C))

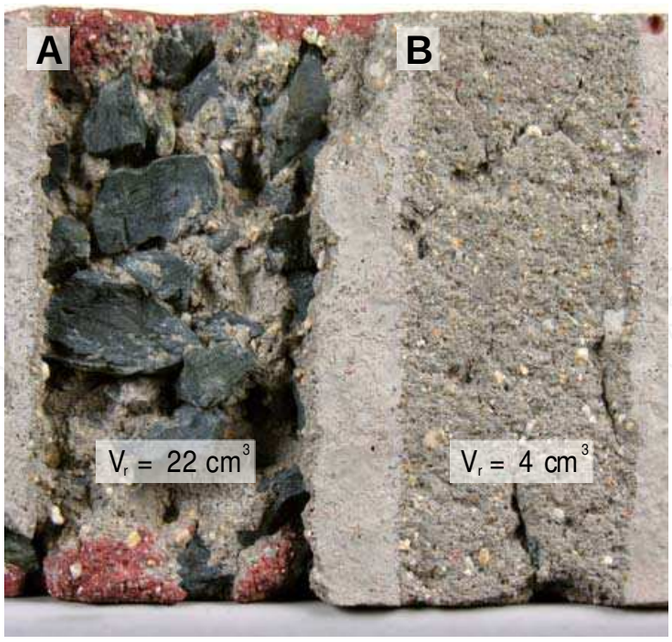

Fig. 14. Comparison of effects of rotating pulsating (A) and rotating continuous (B) water jets on concrete sample (V_r – removed volume, pressure 30 MPa, nozzle diameter 2x1.47 mm, traversing speed 0.5 m.min^{-1}, standoff distance 40 mm (A) and 20 mm (B))

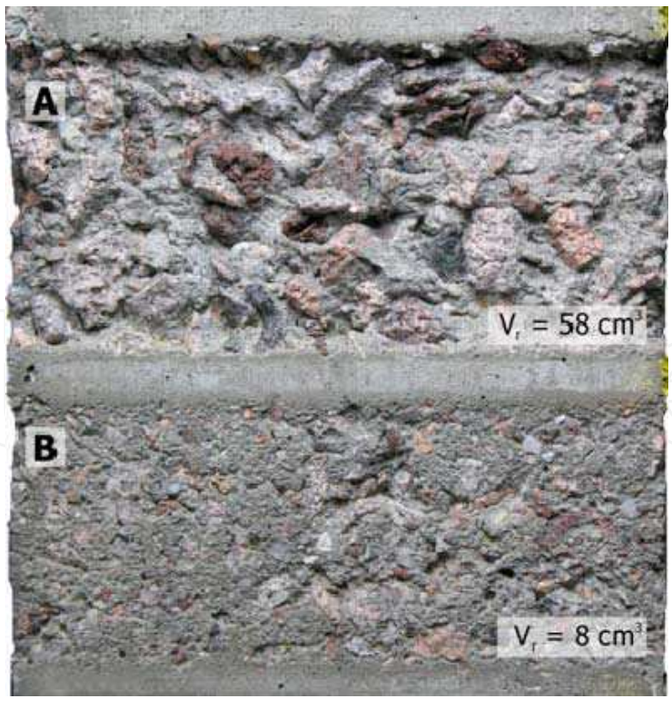

Fig. 15. Comparison of effects of fan pulsating (A) and fan continuous (B) water jets on concrete samples (V_r – removed volume, pressure 30 MPa, equivalent nozzle diameter 2.05 mm, traversing speed 0.2 m.min^{-1}, standoff distance 40 mm)

Results of the measurement of surface roughness characteristics on surfaces created by fan pulsating jets indicate that the characteristics are strongly influenced by both the standoff distance and the operating pressure. An example of the influence of a standoff distance on arithmetic mean roughness (SRa) and average maximum height roughness (SRz) can be seen in Figures 17 and 18, respectively. It should be pointed out that surface roughness (both SRa and SRz) produced by the pulsating fan water jet out of the range of "optimum" standoff distances (where the pulsating jet acts as a continuous jet) correspond to those produced by continuous jets reported by Kunaporn et al. (2009). On the other hand, the fan pulsating water jet produces surfaces with much higher values of the surface roughness (up to 20 times higher) within the "optimum" range of standoff distances (where the pulses are well-developed in the jet) compared to continuous jets.

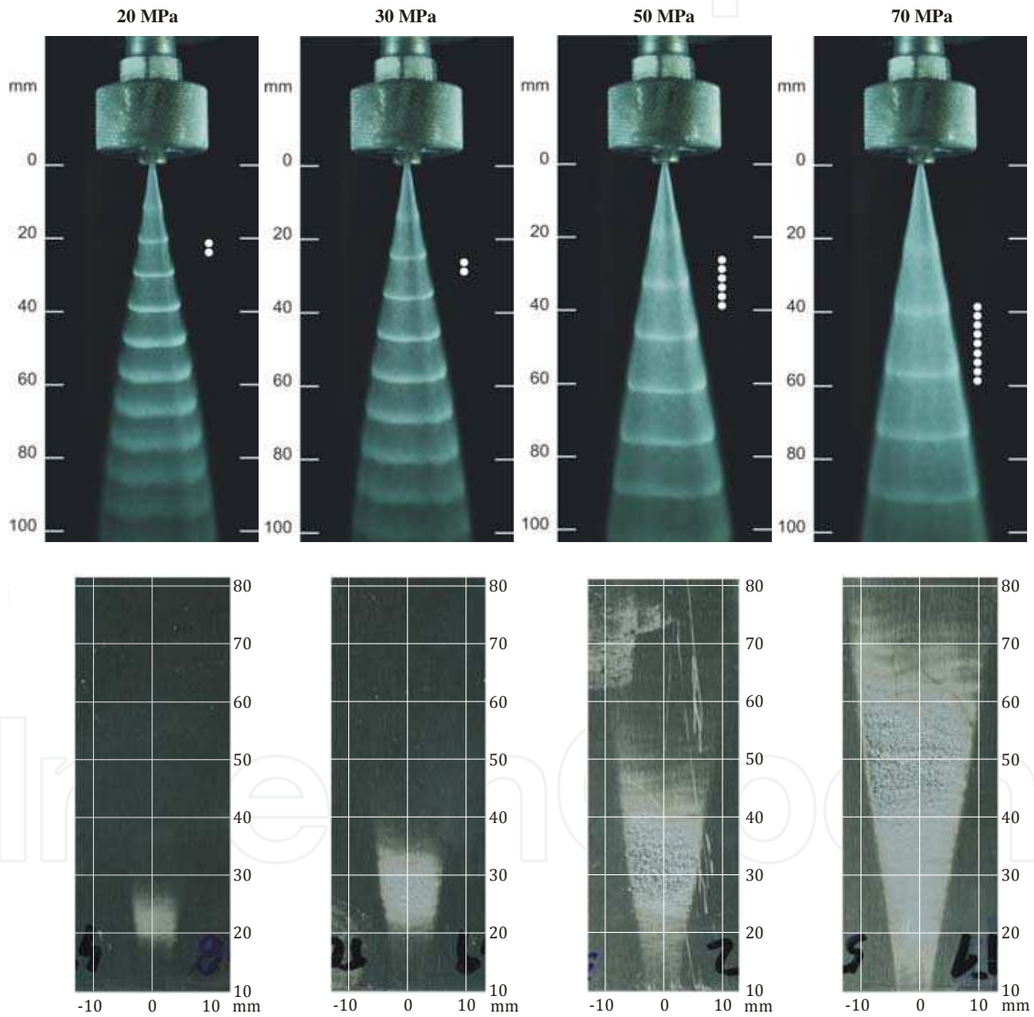

Fig. 16. Top: Pulsating fan water jets generated by nozzle with equivalent of diameter 1.10 mm and spraying angle of 10° at various operating pressures. Scale on the left side of photographs represents standoff distance in millimeters. Dots indicate the range of standoff distances where maximum erosion effects of pulsating fan water jet occur. Bottom: Erosion effects of the above pulsating fan water jets on duralumin samples. Scale on the right side of photographs indicates standoff distance in millimeters; scale on the bottom indicates width in millimeters

Results of the research of effects of pulsating jets on various materials obtained so far indicate that the pulsating jets can be used advantageously for the removal of surface layers of materials and/or "rough" cutting. However, further research will be necessary to be able to use the pulsating water jets in applications of precise cutting.

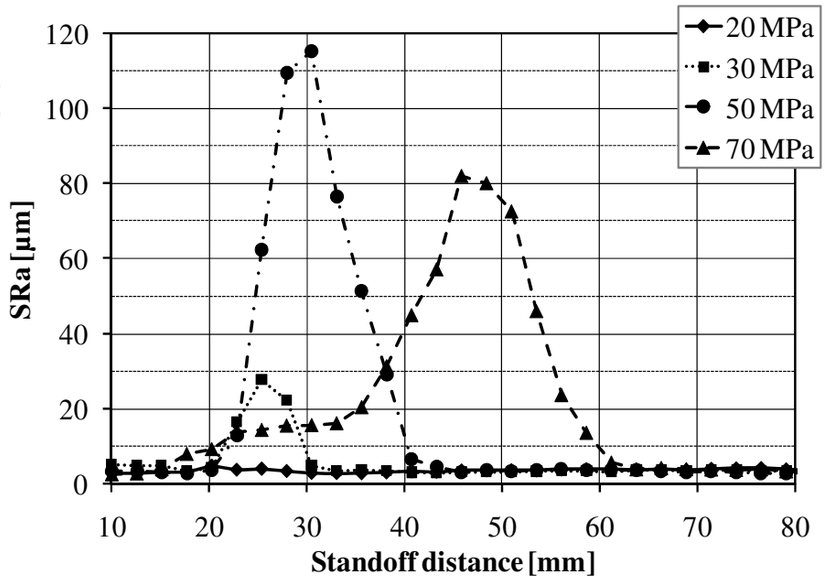

Fig. 17. Influence of a standoff distance on arithmetic mean roughness (SRa) of the surface created by the action of pulsating fan water jet generated by the fan jet nozzle with equivalent of diameter 1.10 mm and spraying angle of 10°

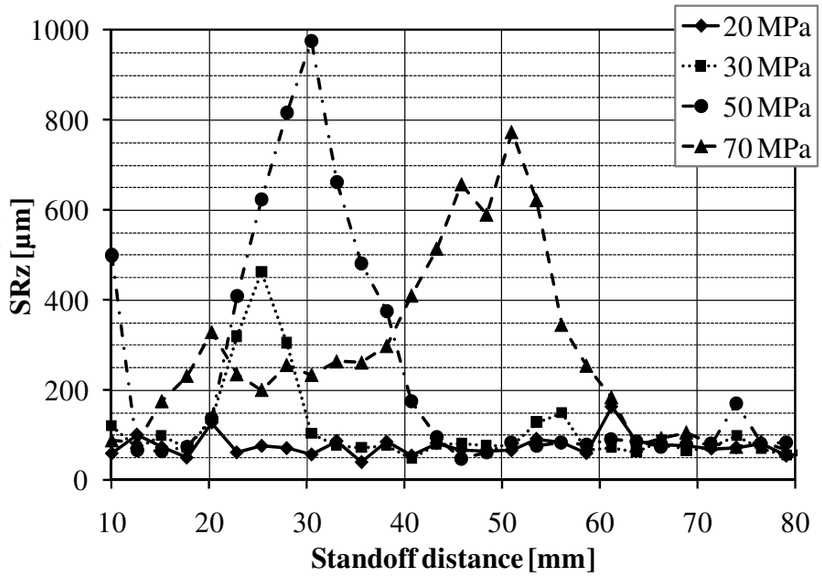

Fig. 18. Influence of a standoff distance on average maximum height roughness (SRz) of the surface created by the action of pulsating fan water jet generated by the fan jet nozzle with equivalent of diameter 1.10 mm and spraying angle of 10°

5. Conclusions

Presented results of the analytical solution and numerical simulation of the transmission of acoustic waves in high-pressure system represent the first step in gaining knowledge regarding processes of generation and propagation of high-frequency pressure pulsations in the liquid under high pressures and their influence on forming and morphology of pulsating liquid jets.

Results obtained from the visualization of pulsating water jets are used in studying of the characteristics of the jets and to verify results obtained from numerical simulation of the process of generating and forming of pulsating water jets. Laboratory and pilot tests of effects of pulsating water jets on various materials showed clearly the potential of pulsating jets to improve the performance of water jetting technology significantly.

It can be concluded that the research presented in the paper contributed to better knowledge of processes occurring in areas of generation and propagation of high-frequency pressure pulsations in the liquid under high pressure, their influence on forming and morphology of pulsating water jets and effects of the jets on materials. However, it is still necessary to further study problems of the efficient transfer of the high-frequency pulsation energy to longer distances in the high-pressure system. This will enable creation of the highly effective pulsating liquid jet with required properties.

6. Acknowledgements

The chapter has been done in connection with project Institute of clean technologies for mining and utilization of raw materials for energy use, reg. no. CZ.1.05/2.1.00/03.0082 supported by Research and Development for Innovations Operational Programme financed by Structural Founds of Europe Union and from the means of state budget of the Czech Republic. Presented work was also supported by the Academy of Sciences of the Czech Republic, project No. AV0Z30860518. Author is thankful for the support.

7. References

Bowden, F. P., & Field, J. E. (1964). The brittle fracture of solids by liquid impact, by solid impact, and by shock. *Proceedings of the Royal Society of London. Series A, Mathematical and Physical Sciences*, Vol. 282, No. 1390, pp. 331-352

de Haller, P. (1933). Untersuchungen über die durch Kavitation hervorgerufenen Korrosionen. *Schweizerische Bauzeitung*, Vol. 101, No. 21& 22, pp. 243-246,260-264

Hancox, N. L., & Brunton, J. H. (1966). The erosion of solids by the repeated impact of liquid drops. *Philosophical Transactions of the Royal Society of London. Series A, Mathematical and Physical Sciences*, Vol. 260, No. 1110, pp. 121-139

Kunaporn, S., Chillman A., Ramulu, M., & Hashish, M. (2009). Effect of waterjet formation on surface preparation and profiling of aluminum alloy. Wear, Vol. 265, No. 1-2, pp. 176-185

Pianthong, K., Zakrzewski, S., Behnia, M., & Milton, B. E. (2003). Characteristics of impact driven supersonic liquid jets. *Experimental thermal and fluid science*, Vol. 27, No. 5, pp. 589-598

Raghavan, C. & Ting, E. (1991). Hyper pressure waterjet cutting of thin sheet metal. *Proceedings of 6th American Water Jet Conference*, pp. 493-504, ISBN 1-880342-00-6, Houston, Texas, August, 1991

Thomas, G. P., & Brunton, J. H. (1970). Drop impingement erosion of metals. *Proceedings of the Royal Society of London. Series A, Mathematical and Physical Sciences*, Vol. 314, No. 1519, pp. 549-565

Tsai, S. C., Luu, P., Tam, P., Roski, G., & Tsai, C. S. (1999). Flow visualization of Taylor-mode breakup of a viscous liquid jet. *Physics of fluids*, Vol. 11, No. 6, pp. 1331-1341

Wong, G. S., & Zhu, S. (1995). Speed of sound in seawater as a function of salinity, temperature and pressure. *Journal of the Acoustical Society of America*, Vol. 97, No. 3, pp. 1732-1736

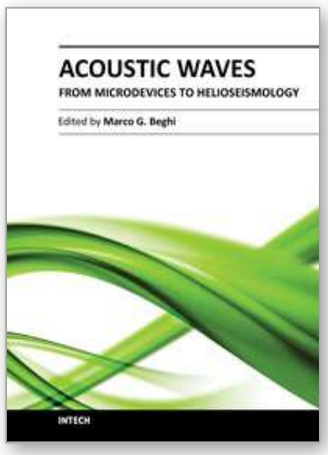

Acoustic Waves - From Microdevices to Helioseismology

Edited by Prof. Marco G. Beghi

ISBN 978-953-307-572-3
Hard cover, 652 pages
Publisher InTech
Published online 14, November, 2011
Published in print edition November, 2011

The concept of acoustic wave is a pervasive one, which emerges in any type of medium, from solids to plasmas, at length and time scales ranging from sub-micrometric layers in microdevices to seismic waves in the Sun's interior. This book presents several aspects of the active research ongoing in this field. Theoretical efforts are leading to a deeper understanding of phenomena, also in complicated environments like the solar surface boundary. Acoustic waves are a flexible probe to investigate the properties of very different systems, from thin inorganic layers to ripening cheese to biological systems. Acoustic waves are also a tool to manipulate matter, from the delicate evaporation of biomolecules to be analysed, to the phase transitions induced by intense shock waves. And a whole class of widespread microdevices, including filters and sensors, is based on the behaviour of acoustic waves propagating in thin layers. The search for better performances is driving to new materials for these devices, and to more refined tools for their analysis.

How to reference

In order to correctly reference this scholarly work, feel free to copy and paste the following:

Josef Foldyna (2011). Use of Acoustic Waves for Pulsating Water Jet Generation, Acoustic Waves - From Microdevices to Helioseismology, Prof. Marco G. Beghi (Ed.), ISBN: 978-953-307-572-3, InTech, Available from: http://www.intechopen.com/books/acoustic-waves-from-microdevices-to-helioseismology/use-of-acoustic-waves-for-pulsating-water-jet-generation

INTECH
open science | open minds

InTech Europe
University Campus STeP Ri
Slavka Krautzeka 83/A
51000 Rijeka, Croatia
Phone: +385 (51) 770 447
Fax: +385 (51) 686 166
www.intechopen.com

InTech China
Unit 405, Office Block, Hotel Equatorial Shanghai
No.65, Yan An Road (West), Shanghai, 200040, China
中国上海市延安西路65号上海国际贵都大饭店办公楼405单元
Phone: +86-21-62489820
Fax: +86-21-62489821

IntechOpen